Supporting Information

Depth-Dependent Defect Manipulation in Perovskites for High-Performance Solar Cells

Yuzhuo Zhang,†[a] Yanju Wang,†[a] Lichen Zhao,*[a] Xiaoyu Yang,[a] Cheng-Hung Hou,*[b] Jiang Wu,[a,f] Rui Su,[a] Shuang Jia,[c] Jing-Jong Shyue,[d] Deying Luo,[e] Peng Chen,[a] Maotao Yu,[a] Qiuyang Li,[a] Lei Li,[a] Qihuang Gong,[a,f,g] and Rui Zhu*[a,f,g]

[a.] State Key Laboratory for Artificial Microstructure and Mesoscopic Physics, School of Physics, Frontiers Science Center for Nano-optoelectronics & Collaborative Innovation Center of Quantum Matter, Peking University, Beijing 100871, China. E-mail: lczhao@pku.edu.cn; iamzhurui@pku.edu.cn

[b.] Research Center for Applied Sciences, Academia Sinica, Taipei 11529, Taiwan. E-mail: chhou@gate.sinica.edu.tw

[c.] International Center for Quantum Materials, School of Physics, Peking University, Beijing 100871, China.

[d.] Department of Materials Science and Engineering, National Taiwan University, Taipei 10617, Taiwan.

[e.] Department of Materials Science and Engineering, University of Toronto, Toronto M5G 3E4, Canada.

[f.] Peking University Yangtze Delta Institute of Optoelectronics, Nantong, Jiangsu, 226010, China.

[g.] Collaborative Innovation Center of Extreme Optics, Shanxi University, Taiyuan, Shanxi 030006, China.

† These authors contributed equally to this work.

Experimental Section

Materials and Reagents： Lead iodide (PbI_2, 99.99%) was purchased from Tokyo Chemical Industry Co., Ltd (TCI, Japan). The black $FAPbI_3$ crystal was synthesized according to the procedure reported in the literature. [1] Guanidinium iodide (GuaI, >98.0%), 4-*tert*-butyl-phenylmethylammonium iodide (tBPMAI, >98.0%), ethylamine hydroiodide (EAI, >98.0%), phenethylammonium iodide (PEAI, >98.0%) and methylammonium chloride (MACl, >98.0%) were received from Xi'an Polymer Light Technology Corp (China). Ultra-dry solvents such as dimethylformamide (DMF, >99.8%), dimethyl sulfoxide (DMSO, >99.8%), isopropanol (IPA, >99.5%) and chlorobenzene (CB, >99.8%), acetonitrile (ACN, >99.8%), ethyl alcohol (EtOH, >99.0%) were purchased from Acros. Li-bis(trifluoromethanesulfonyl)imide Li-TFSI, >98.0%), acetyl acetone (>98.0%), 4-*tert*-butylpyridine (TBP, >98.0%), and titanium diisopropoxide bis(acetylacetonate) 75% wt in IPA were purchased from Sigma-Aldrich. Titanium dioxide paste (30 NRD) and formamidinium iodide (FAI, >98.0%) were purchased from Greatcell LTD, Australia. 2,2',7,7'-tetrakis(*N,N*-di-p-methoxyphenylamine)-9,9'-spirobifluorene (Spiro-OMeTAD, 99.8%) was purchased from Ningbo Borun New Material Co., Ltd. All the chemicals were used as received without further purification. Conductive glasses, fluorine-doped tin oxide (FTO, 7 Ω sq^{-1}), were purchased from OPV Tech Co. Ltd, China.

Solar Cell Fabrication： For mesoscopic structure solar cells, FTO conductive glasses were cleaned sequentially using diluted detergent aqueous solution, deionized water, acetone, and IPA by sonicating for 20 minutes for each solvent. After drying, the compact TiO_2 (c-TiO_2) layer was deposited by spray pyrolysis (O_2 as the carrier gas) of 9-ml ethanol solution containing 0.6-ml titanium diisopropoxide bis(acetylacetonate) solution and 0.4-ml acetylacetone on the top of the preheated FTO substrates at 450 °C in air. After cooling down

to room temperature, a mesoscopic TiO_2 (m-TiO_2) layer was spin-coated by a diluted solution of 30 NRD paste (mass ratio, paste:EtOH = 1:6) at 4000 rpm with the acceleration of 2000 rpm s^{-1}, followed by annealing in ambient conditions (relative humidity of ~40%) at 450 °C for 60 minutes. The resultant FTO/c-TiO_2/m-TiO_2 substrates were then cleaned with UV ozone treatment for 10 minutes before perovskite precursor coating. The perovskite films were deposited on the substrates using a one-step antisolvent-assisted method. For the control perovskite film, 1.8 M $FAPbI_3$/DMF-DMSO (V_{DMF}:V_{DMSO} = 1:6) precursor solution with 35 mol% MACl was deposited by spin coating at 1000 and 5000 rpm for 10 and 20 seconds, respectively. During the 5000-rpm spin coating stage, 100-μL CB was poured on the spinning substrate at the 15th second. Then, the fresh wet films were annealed at 150 °C for 15 min in ambient environment (ca. relative humidity of 40%). The hole transport material (HTM) solution was spin-coated on the perovskite film at 4000 rpm for 20 seconds with an acceleration rate of 2000 rpm s^{-1}. The HTM solution was prepared by dissolving 72.3-mg Spiro-OMeTAD, 28.8-μL TBP and 17.5-μL Li-TFSI solution (520 mg mL^{-1} in ACN) into 1-mL CB. Finally, an 80-nm-thick Au layer and a 125-nm-thick MgF_2 anti-reflective layer were thermally deposited under high vacuum on the top of HTL and back of glass substrates, respectively. For single GuaI or tBPMAI treatment, 90-μL solution (5 mg ml^{-1} in IPA) was spin-coated on the surface of the perovskite film at 5000 r.p.m for 30 seconds followed by 100 °C annealing on a hot plate for 5 minutes. The binary GuaI/tBPMAI post treatment follows the same procedure as the single GuaI or tBPMAI treatment except that the solution was prepared by directly mixing GuaI-based solution and tBPMAI-based solution with varied mass ratios. The optimal GuaI/tBPMAI solution is composed of 1.67 mg/ml GuaI and 3.33 mg/ml tBPMAI in IPA.

Characterizations： The ToF-SIMS analysis was conducted using a PHI TRIFT V nanoTOF (ULVAC-PHI, Japan) system via the dual beam slice-and-view analysis scheme. During the data acquisition, a pulsed 20 kV C_{60}^+ primary ion beam with a pulse frequency of

approximately 8200 Hz and a pulse length of 15 ns was utilized to generate the secondary ions. The beam current of the C_{60}^+ primary ion beam was 0.15 nA-DC. All the ToF-SIMS results were obtained from a 50 μm × 50 μm area on the sample surface. The ejected secondary ions were accelerated by a sample bias of 3 kV, so the secondary ions could gain enough kinetic energy to reach the SIMS detector. All the tracked secondary ions were positively charged monovalence fragments. Information regarding the formula and mass of the tracked ion were stated in the caption of each ToF-SIMS figure. Pulsed 10 V electron and 10 V Ar^+ flooding was simultaneously applied during the data acquisition to compensate the surface charge. The signal intensities were normalized by the corresponding total ion intensities in the ToF-SIMS depth profiles so current fluctuations of the primary ion beam could be compensated. During the sputtering, a 20 kV C_{60}^+ sputter ion beam was applied to remove the surface material. The beam current of the C_{60}^+ sputter beam was 1 nA-DC. The C_{60}^+ sputter beam was rastered over a large 500 μm × 500 μm area to avoid the crater-edge effect that might interfere with the observations. Field-emission scanning electron microscopy (SEM, FEI Nova Nano SEM 430) was used to investigate the surface morphology, with an accelerating voltage of 10 kV. AFM topography of the perovskite surfaces were acquired a SPM system (Veeco Innova SPM) under the tapping mode. The X-ray diffraction (XRD) samples were characterized by Mini Flex 600 (Rigaku, Japan). UV-vis absorption spectra were measured using a spectrophotometer (UH4150, Hitachi, Japan). The steady-state photoluminescence (PL) and time-resolved photoluminescence (TRPL) were performed on an Edinburgh Instruments FLS1000 photoluminescence spectrometer (Edinburg, UK) additionally equipped with an integrating sphere, and all TRPL-related tests were measured under the excitation wavelength of 450 nm after 150-second illumination. The fluence of laser is 0.18 nJ cm^{-2} per pulse. The cross-sectional confocal PL mappings were measured by a confocal fluorescence microscope (ISS Q2 FLIM/FFS, ISS Inc.) under excitation wavelength of 488 nm. X-ray photoelectron spectrometer (Thermo-Fisher

Escalab 250Xi using Al Kα X-ray) was used to acquire the surface chemical environment changes of perovskite films. The photocurrent-voltage (*J-V*) characteristics of the solar cells with an active area of 0.103 cm^2 were measured using a Keithley 2400 Source Meter under illumination of a simulated sunlight (AM1.5 G, 100 mW cm^{-2}) using a 150 W Class AAA solar simulator (XES-40S1, SAN-EI). A non-reflective mask with an aperture area of 0.09 cm^2 was used. The light intensity was calibrated by a standard monocrystalline silicon diode with a KG-5 filter before test. All the tested perovskite films were prepared on FTO/c-TiO_2/m-TiO_2 substrates according to the device fabrication method mentioned above.

Figures and Tables

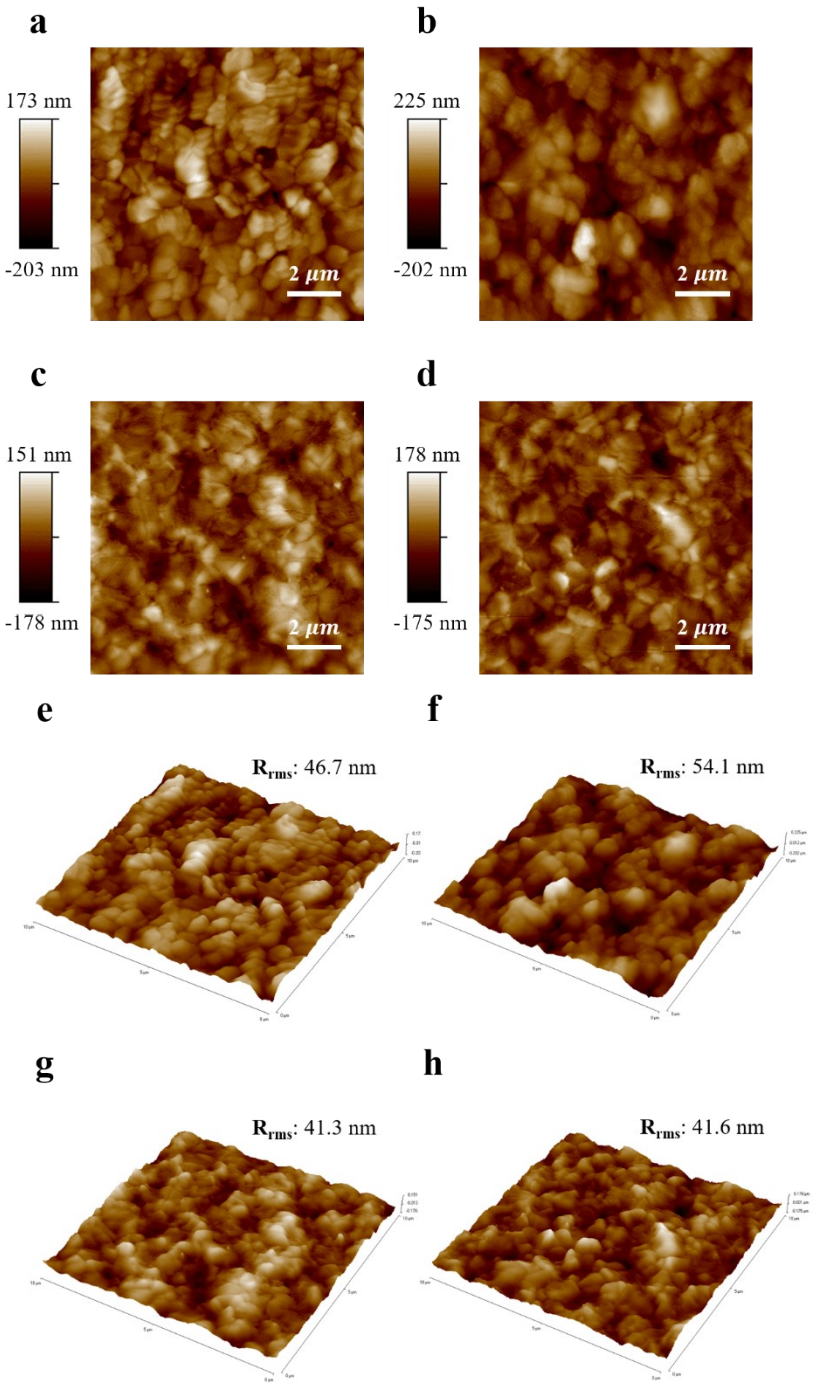

Fig. S1. (a-d) 2D and (e-h) 3D surface topographies of (a, e) control, (b, f) GuaI-treated, (c, g) tBPMAI-treated, and (d, h) GuaI/tBPMAI-treated perovskite film acquired by AFM.

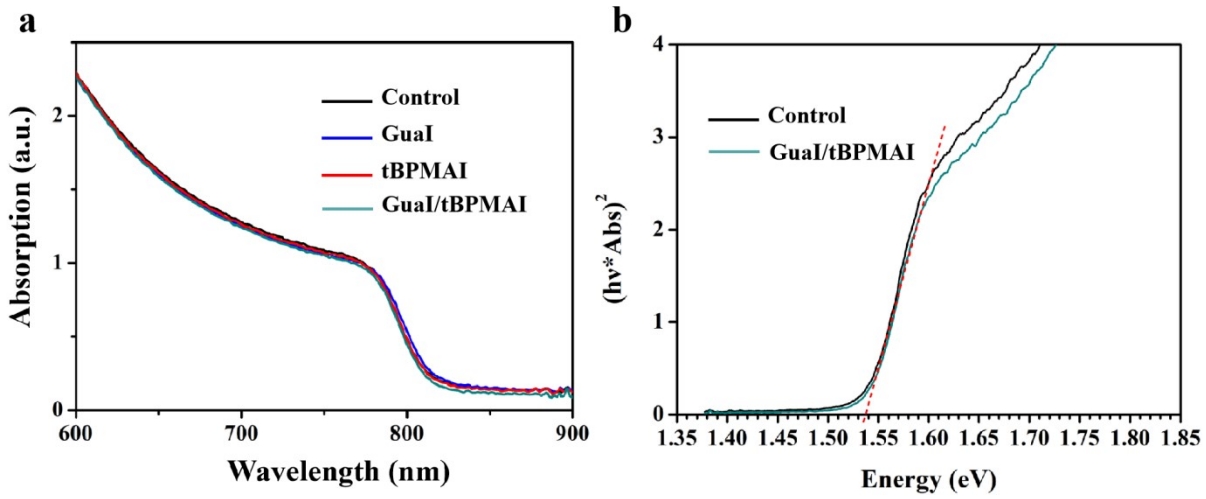

Fig. S2. Ultraviolet-visible (UV-vis) absorption spectra (a) and corresponding Tauc plots (b) of the control and GuaI/tBPMAI-treated perovskite films. The optical bandgaps of perovskites are estimated to be around 1.535 eV.

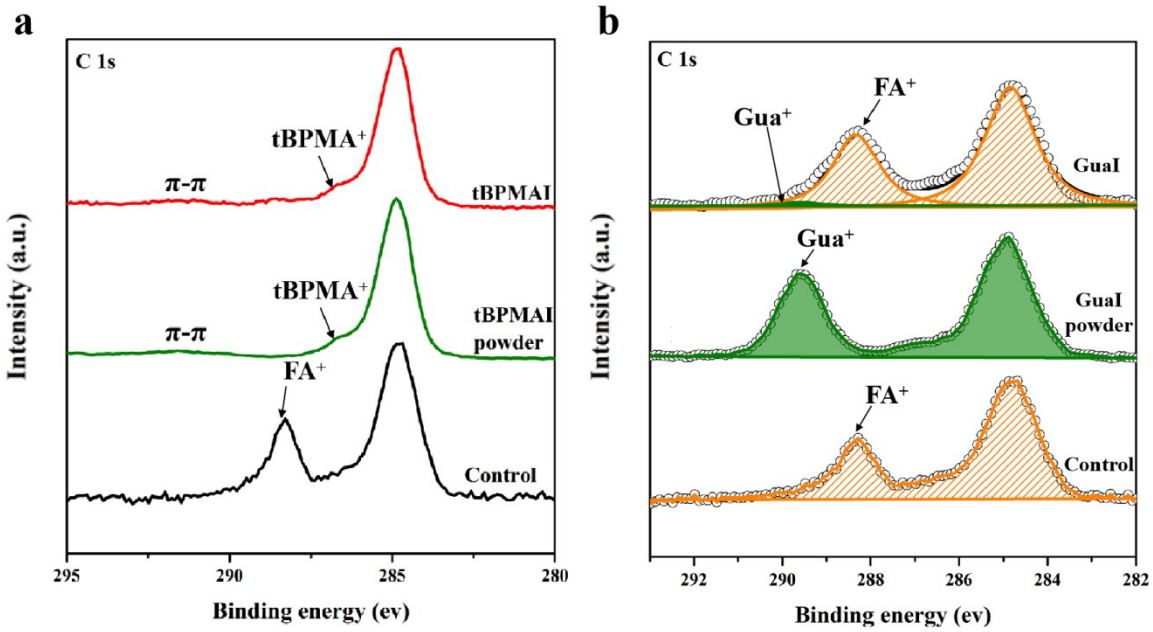

Fig. S3. C 1s characteristic spectra of the perovskite films treated without or with (a) tBPMAI and (b) GuaI and the corresponding powder samples of the ammonium salts.

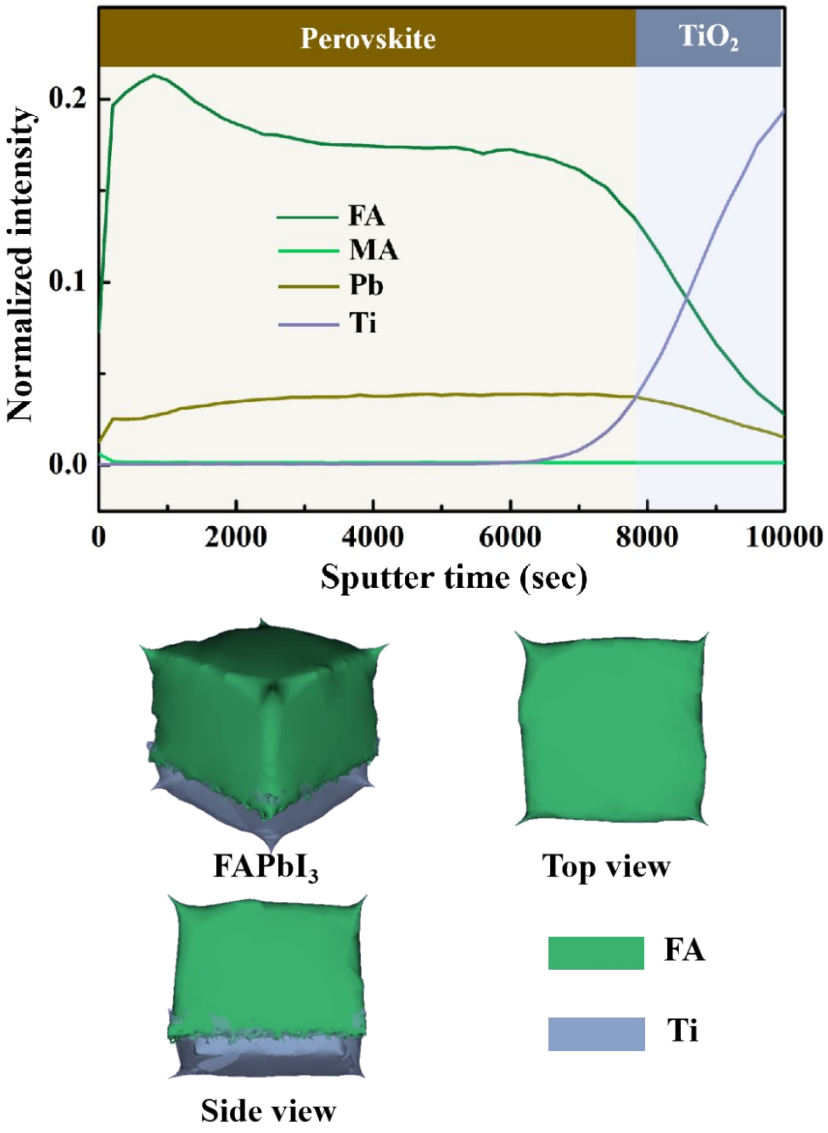

Fig. S4. Depth profiles and reconstructed 3D images of the control perovskite ($FAPbI_3$) film deposited on FTO/c-TiO_2/m-TiO_2 substrate. The tracked ions are all positively charged monovalence fragments and the tracked m/z values are 45 ($CH(NH_2)_2^+$) for FA, 32 ($CH_3NH_3^+$) for MA, 208 (Pb^+) for Pb, and 48 (Ti^+) for Ti.

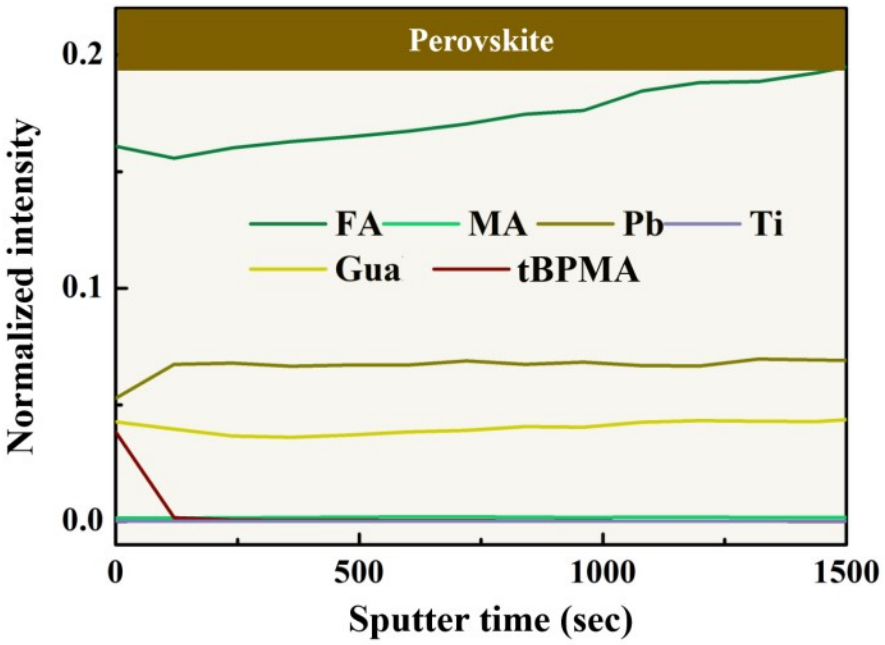

Fig. S5. The amplified depth profiles showing the component distribution near the top-surface region in Figure 2a. The tracked ions are all positively charged monovalence fragments and the tracked m/z values are 45 ($CH(NH_2)_2^+$) for FA, 32 ($CH_3NH_3^+$) for MA, 208 (Pb^+) for Pb, 48 (Ti^+) for Ti, 60 ($C(NH_2)_3^+$) for Gua, and 147 ($C_4H_9C_6H_4CH_2^+$) for tBPMA.

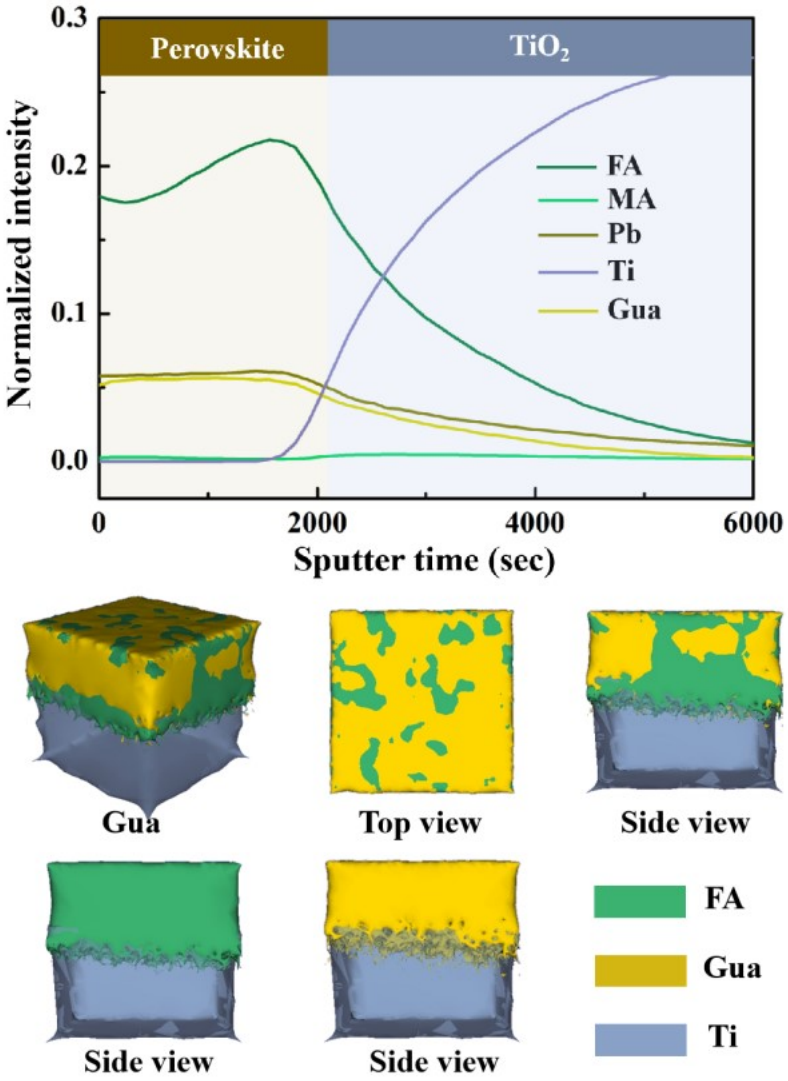

Fig. S6. Depth profiles and reconstructed 3D images of unitary GuaI-treated perovskite film deposited on FTO/c-TiO_2/m-TiO_2 substrate. The tracked ions are all positively charged monovalence fragments and the tracked m/z values are 45 ($CH(NH_2)_2^+$) for FA, 32 ($CH_3NH_3^+$) for MA, 208 (Pb^+) for Pb, 48 (Ti^+) for Ti, and 60 ($C(NH_2)_3^+$) for Gua.

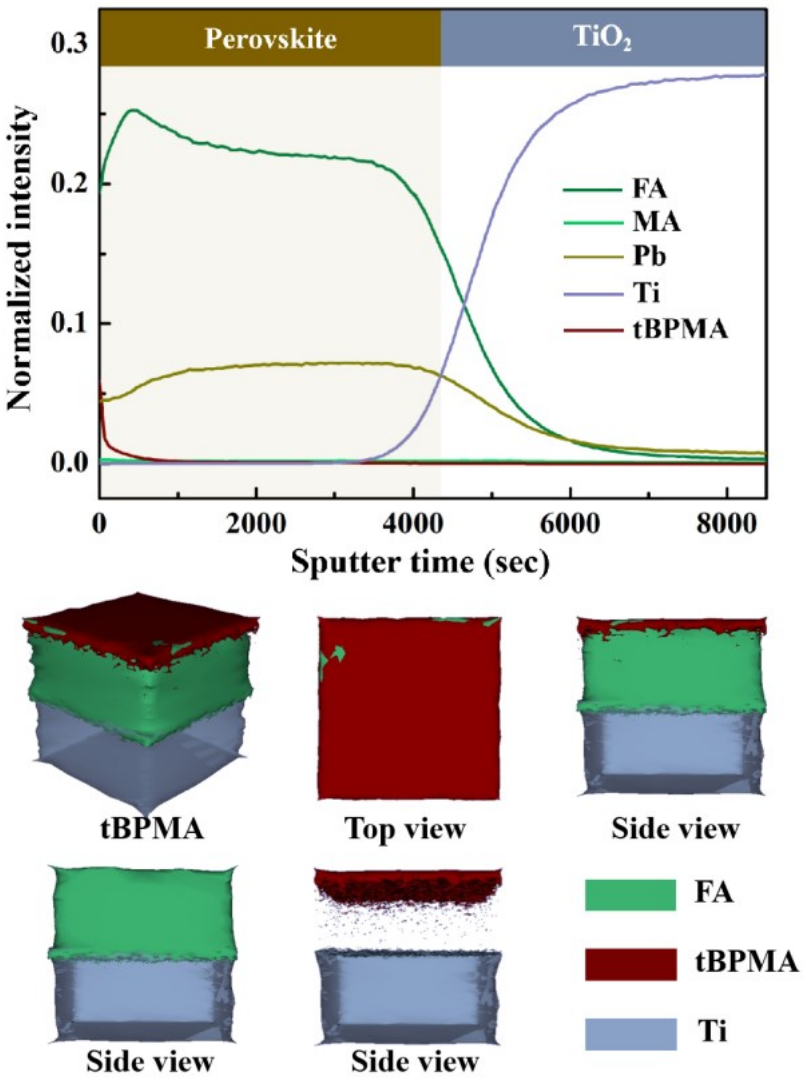

Fig. S7. Depth profiles and reconstructed 3D images of the unitary tBPMAI-treated perovskite film deposited on FTO/c-TiO_2/m-TiO_2 substrate. The tracked ions are all positively charged monovalence fragments and the tracked m/z values are 45 ($CH(NH_2)_2^+$) for FA, 32 ($CH_3NH_3^+$) for MA, 208 (Pb^+) for Pb, 48 (Ti^+) for Ti, and 147 ($C_4H_9C_6H_4CH_2^+$) for tBPMA.

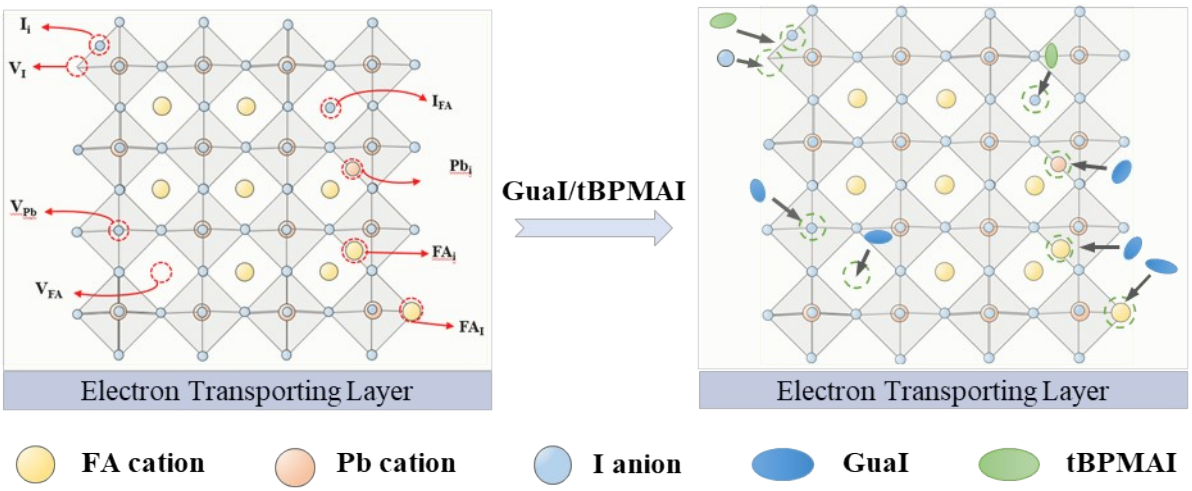

Fig. S8. Schematic for the manipulation of various kinds of defects in the $FAPbI_3$ perovskite films by the binary GuaI/tBPMAI passivators. The V_{Pb}, V_I, V_{FA}, FA_I, I_{FA}, Pb_I, I_i, FA_i and Pb_i denote the Pb vacancy, I vacancy, FA vacancy, FA-I antisite, I-FA antisite, Pb-I antisite, I interstitial, FA interstitial and Pb interstitial defects, respectively.

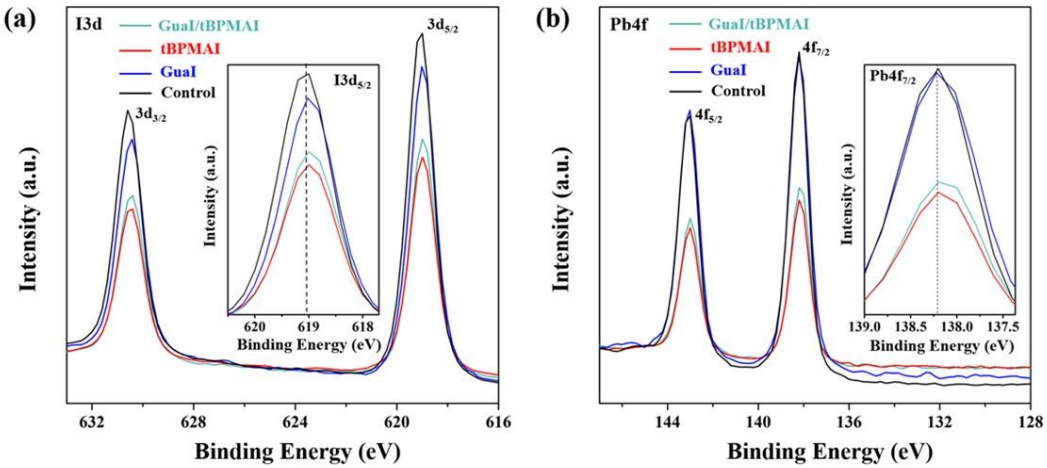

Fig. S9. High-resolution (a) Pb4f and (b) I3d XPS spectra acquired from the control, unitary GuaI-treated, unitary tBPMAI-treated and binary GuaI/tBPMAI-treated films.

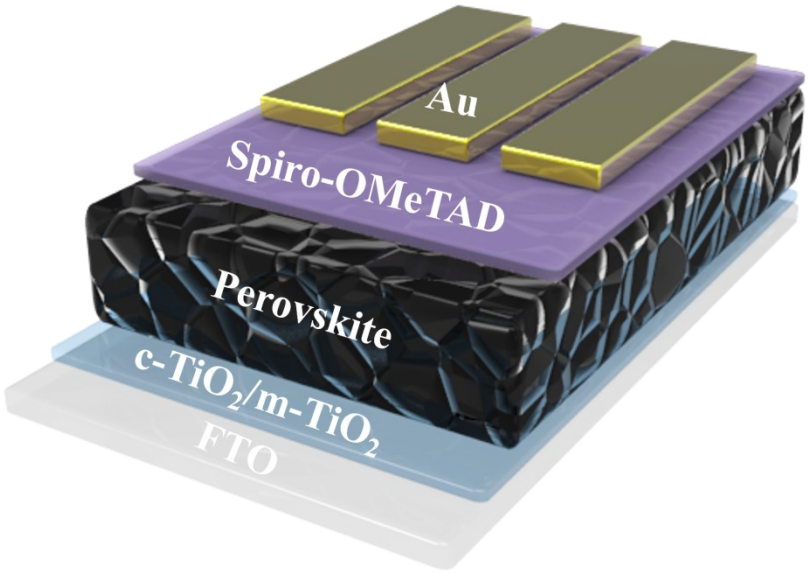

Fig. S10. The device architecture of the regular-structure PSCs. The perovskite film is deposited on FTO/c-TiO_2/m-TiO_2 substrate, and then covered with a layer of 2,2',7,7'-tetrakis[*N*,*N*-di-p-methoxyphenylamine]-9,9'-spirobifluorene (Spiro-OMeTAD) and gold (Au) electrode.

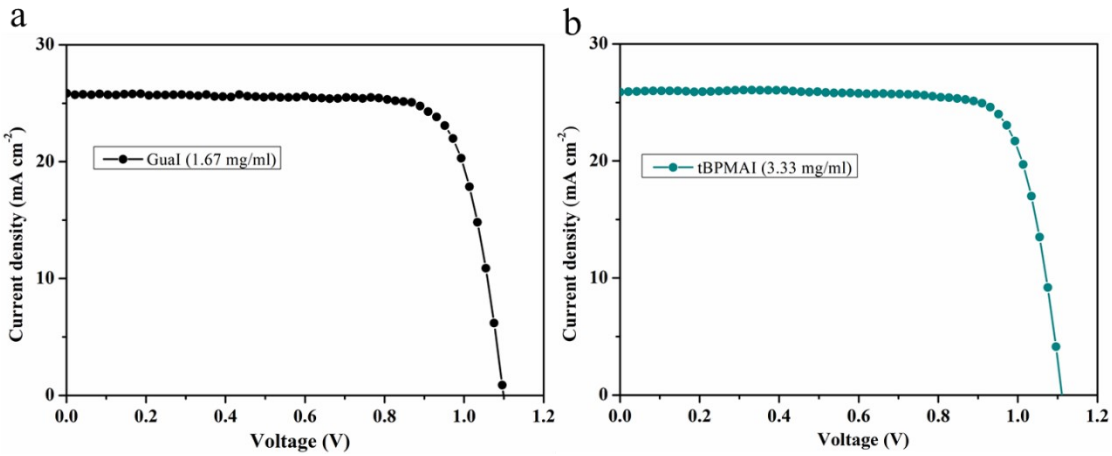

Fig. S11. *J-V* curves of (a) GuaI (1.67 mg/ml)- and (b) tBPMAI (3.33 mg/ml)-treated PSCs.

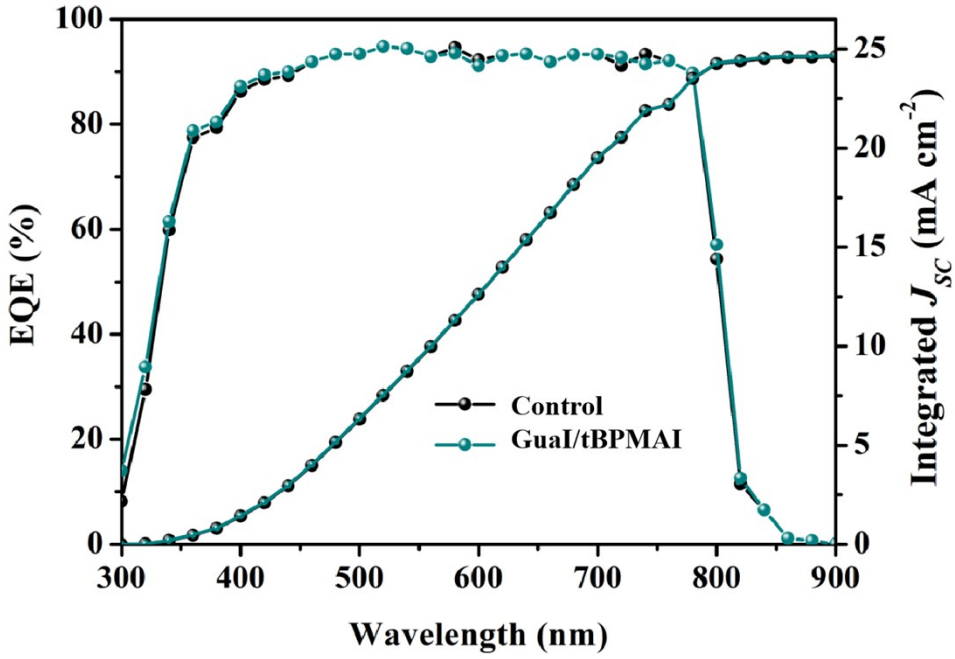

Fig. S12. External quantum efficiencies (EQEs) and corresponding integrated current densities of the control and GuaI/tBPMAI-treated PSCs.

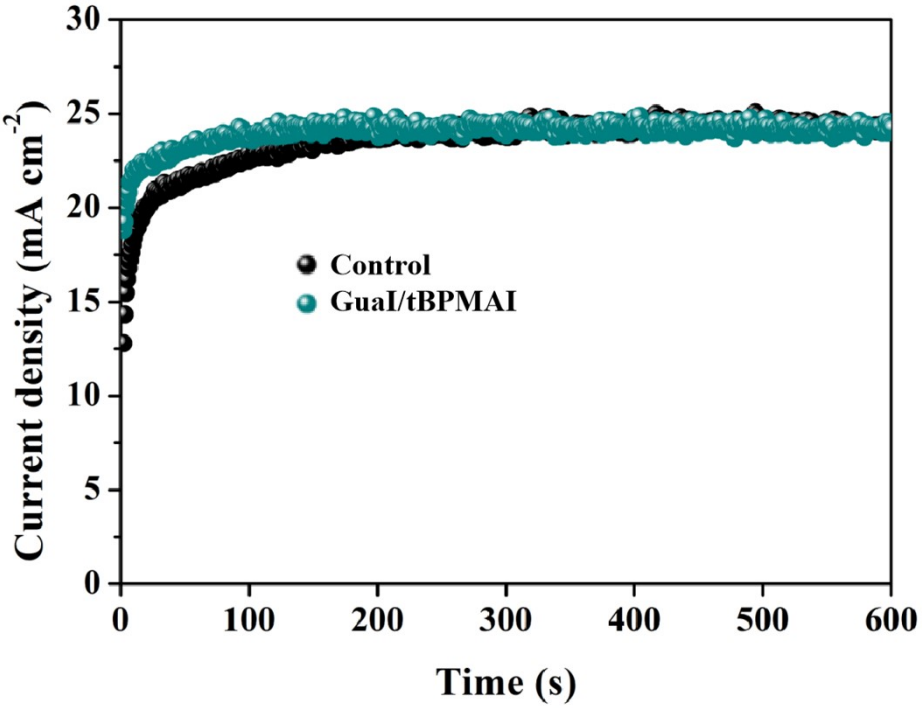

Fig. S13. The stabilized current densities of the control and GuaI/tBPMAI-treated PSCs, which are measured under the voltages at maximum power points of 0.889 V and 0.993 V in ambient air under AM1.5 G illumination, respectively.

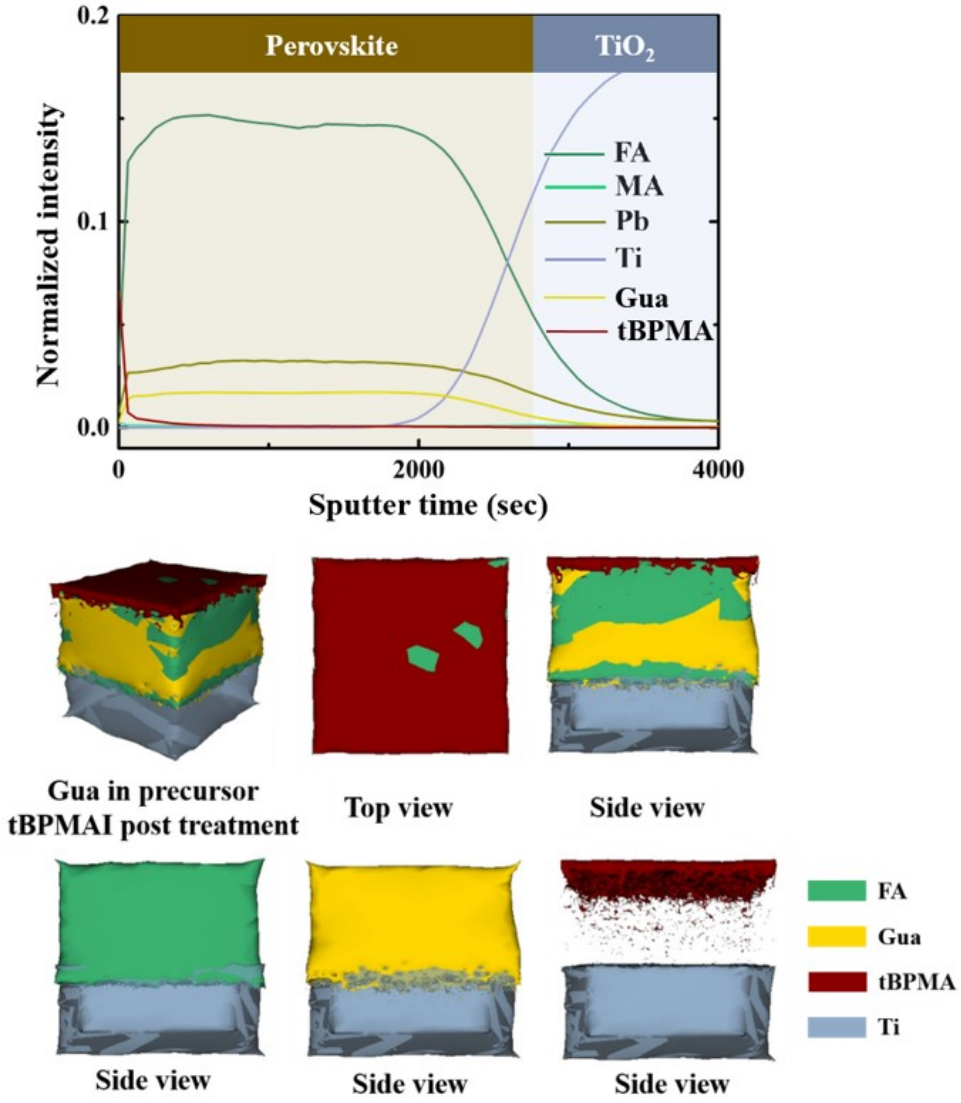

Fig. S14. Depth profiles and reconstructed 3D images of the perovskite film, which was deposited using the precursor solution with GuaI additive and sequentially followed by additional tBPMAI post-treatment. The sample architecture is FTO/c-TiO_2/m-TiO_2/perovskite. The tracked ions are all positively charged monovalence fragments and the tracked m/z values are 45 ($CH(NH_2)_2^+$) for FA, 32 ($CH_3NH_3^+$) for MA, 208 (Pb^+) for Pb, 48 (Ti^+) for Ti, 60 ($C(NH_2)_3^+$) for Gua, and 147 ($C_4H_9C_6H_4CH_2^+$) for tBPMA.

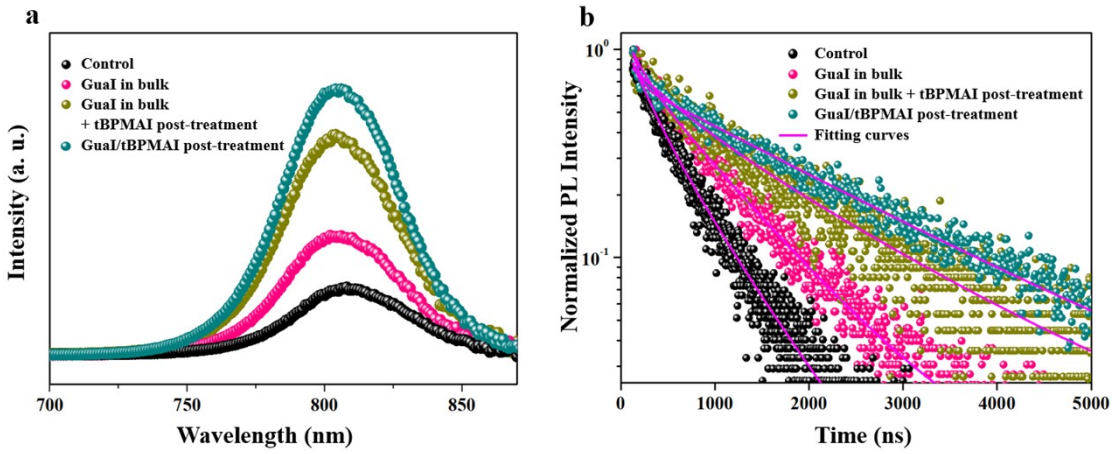

Fig. S15. (a) Steady-state PL and (b) TRPL spectra of the perovskite films.

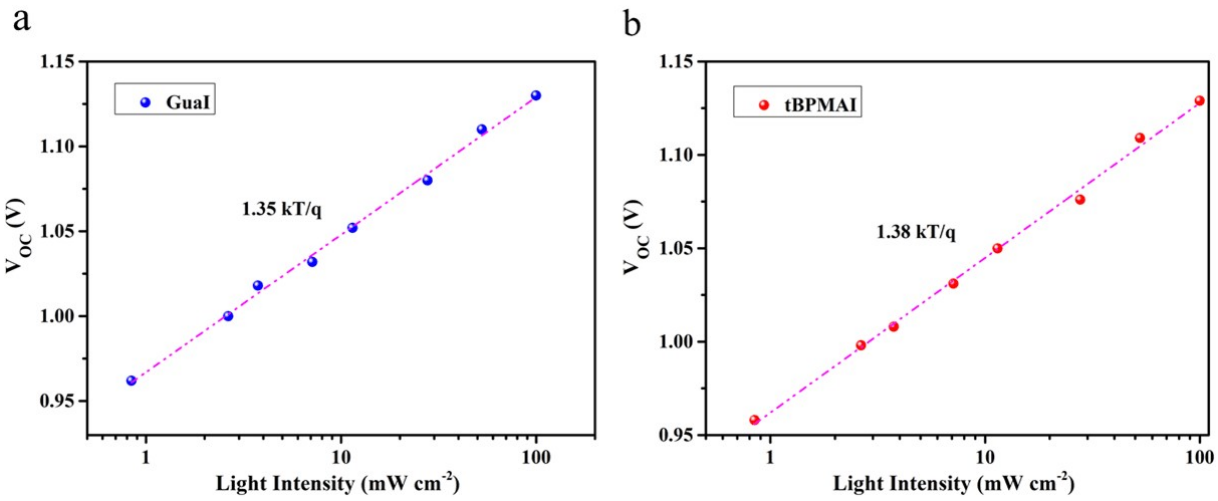

Fig. S16. The logarithmic scale of the V_{OC} versus incident light intensity for for (a) GuaI- and (b) tBPMAI- treated devices.

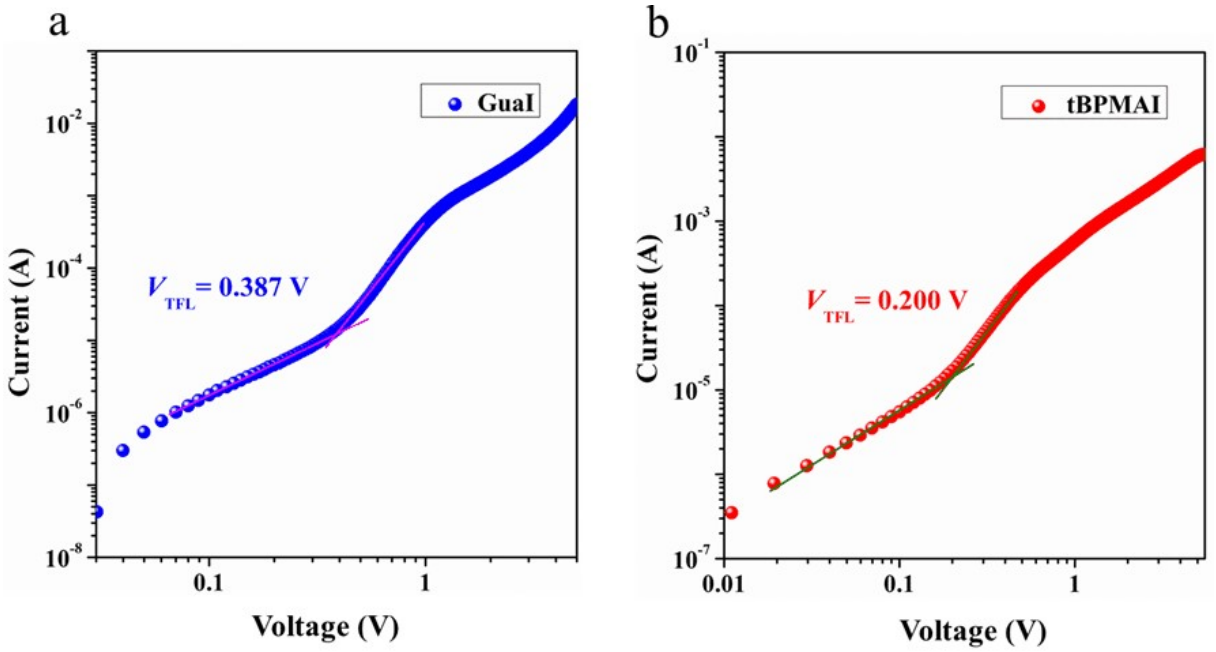

Fig. S17. *I-V* curves of the hole-only devices for (a) GuaI- and (b) tBPMAI- treated devices.

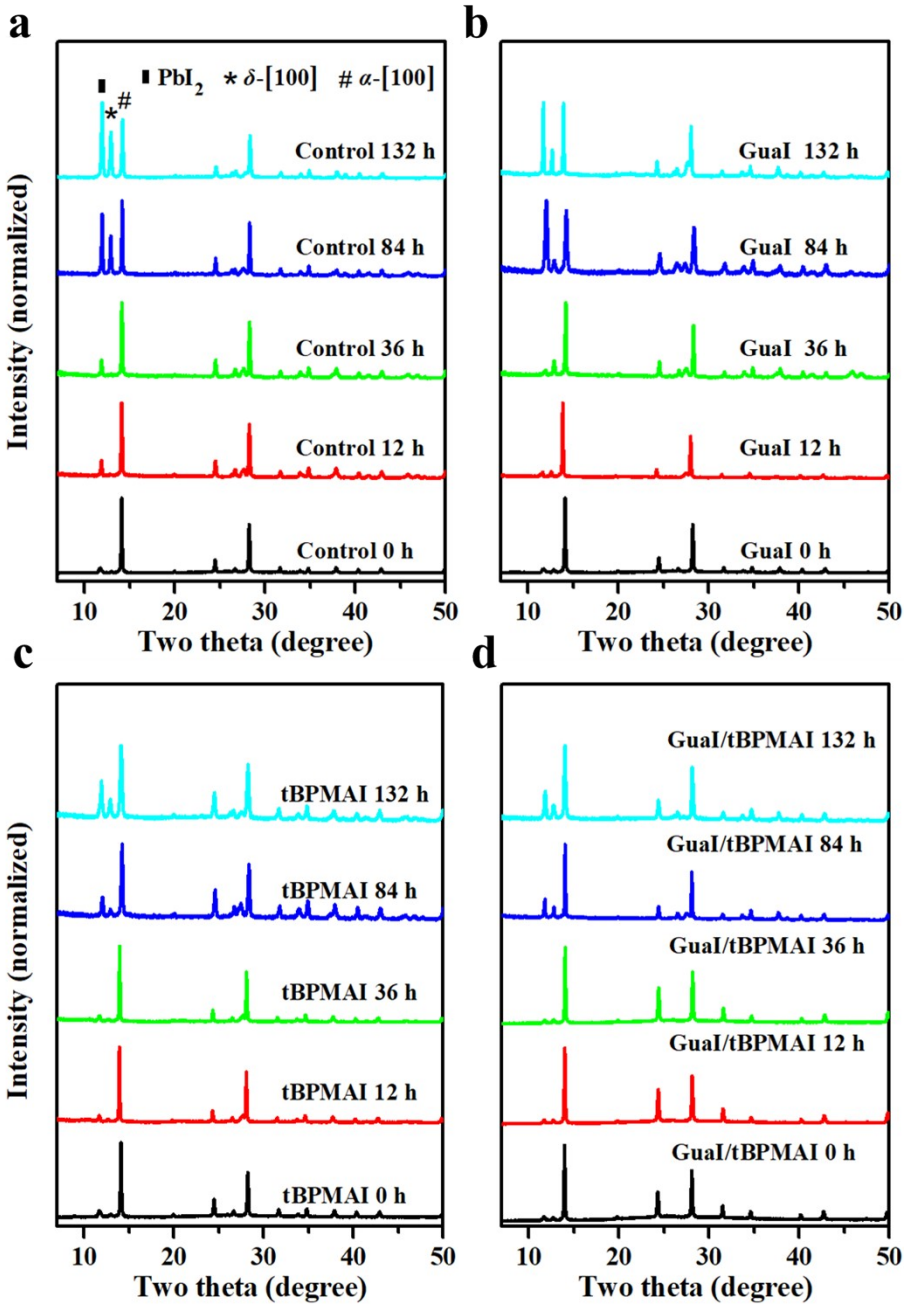

Fig. S18. The XRD patterns of control, GuaI-, tBPMAI-, and GuaI/tBPMAI-treated $FAPbI_3$ films with different storage durations at 85 °C in a N_2-filled glovebox. For unitary GuaI or tBPMAI treatment, the concentration of the post-treatment solution is 5 mg/ml of in IPA, while the optimized GuaI/tBPMAI solution is composed of 1.67 mg/ml GuaI and 3.33 mg/ml tBPMAI in IPA.

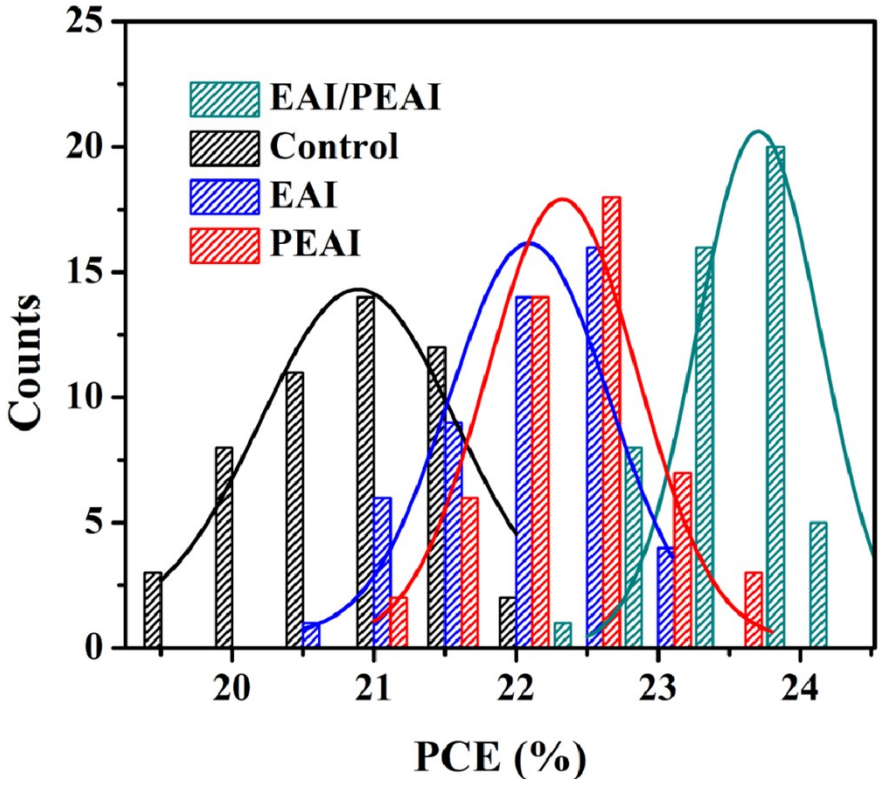

Fig. S19. Statistical results of PCEs fitted with Gaussian distributions from a batch of 50 devices for control, EAI, PEAI and EAI/PEAI-based PSCs, repsectively.

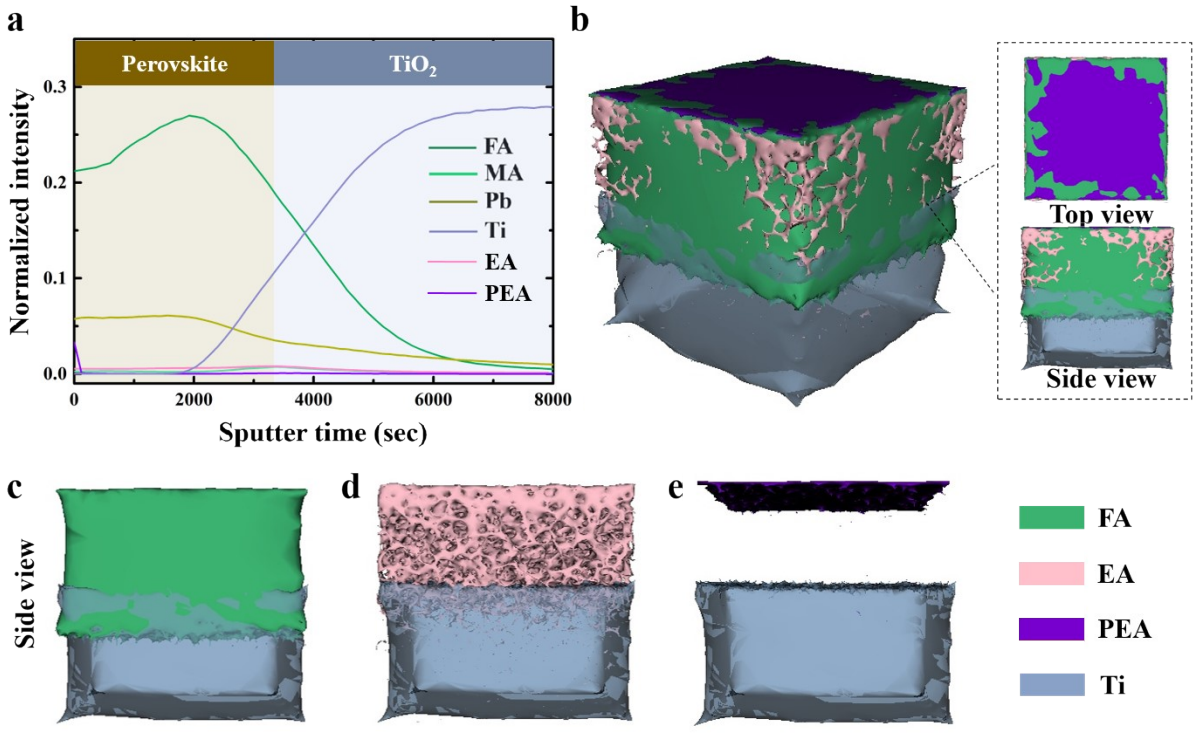

Fig. S20. (a) ToF-SIMS depth profiles and (b) ToF-SIMS 3D images of the binary EAI/PEAI-treated perovskite film deposited on FTO/c-TiO_2/m-TiO_2 substrate. (c, d, e) Side-view 3D images of the solely depicted FA, EA and PEA distribution, respectively. The tracked ions are all positively charged monovalence fragments and the tracked m/z values are 45 ($CH(NH_2)_2^+$) for FA, 32 ($CH_3NH_3^+$) for MA, 208 (Pb^+) for Pb, 48 (Ti^+) for Ti, 46 ($C_2H_5NH_3^+$) for EA, and 91 ($C_6H_5CH_2^+$) for PEA.

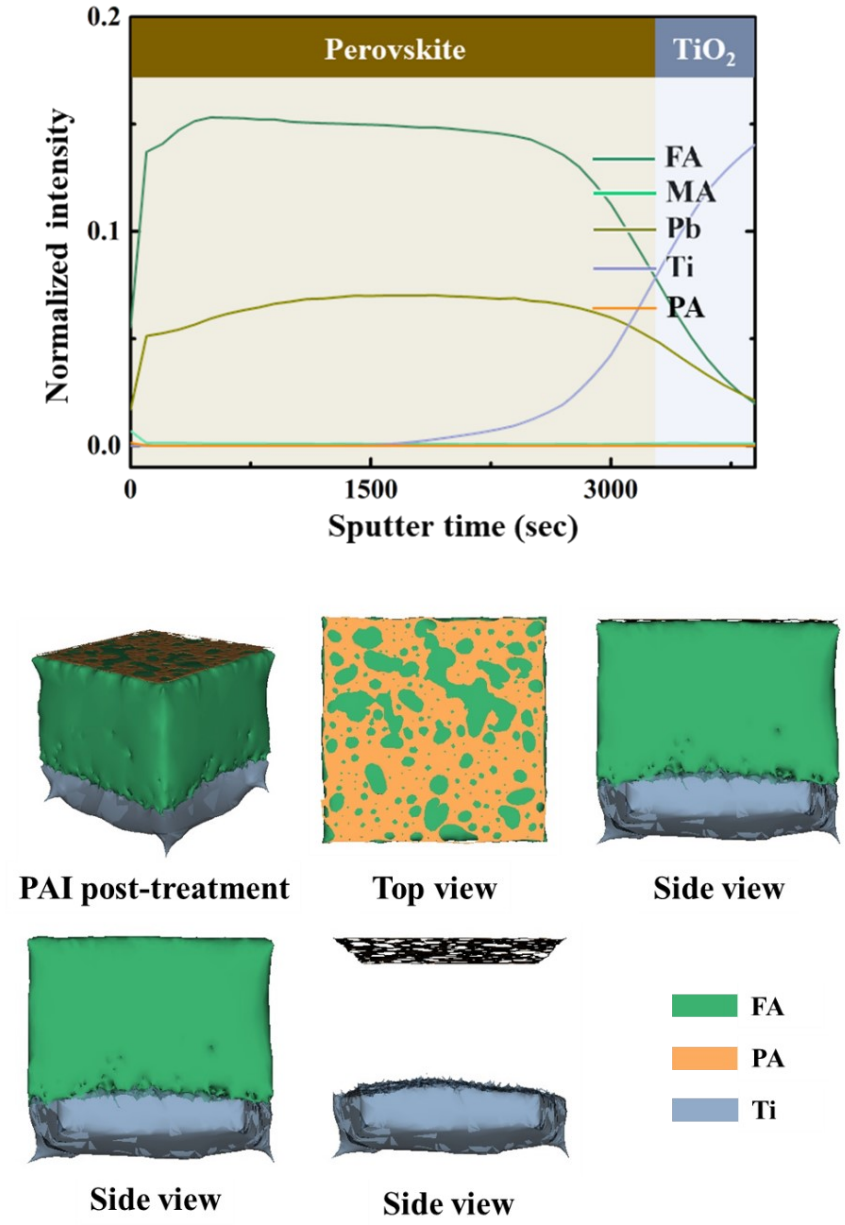

Fig. S21. Depth profiles and reconstructed 3D images of the unitary PAI-treated perovskite film deposited on FTO/c-TiO_2/m-TiO_2 substrate. The tracked ions are all positively charged monovalence fragments and the tracked m/z values are 45 ($CH(NH_2)_2^+$) for FA, 32 ($CH_3NH_3^+$) for MA, 208 (Pb^+) for Pb, 48 (Ti^+) for Ti, and 94 ($C_6H_5NH_3^+$) for PA.

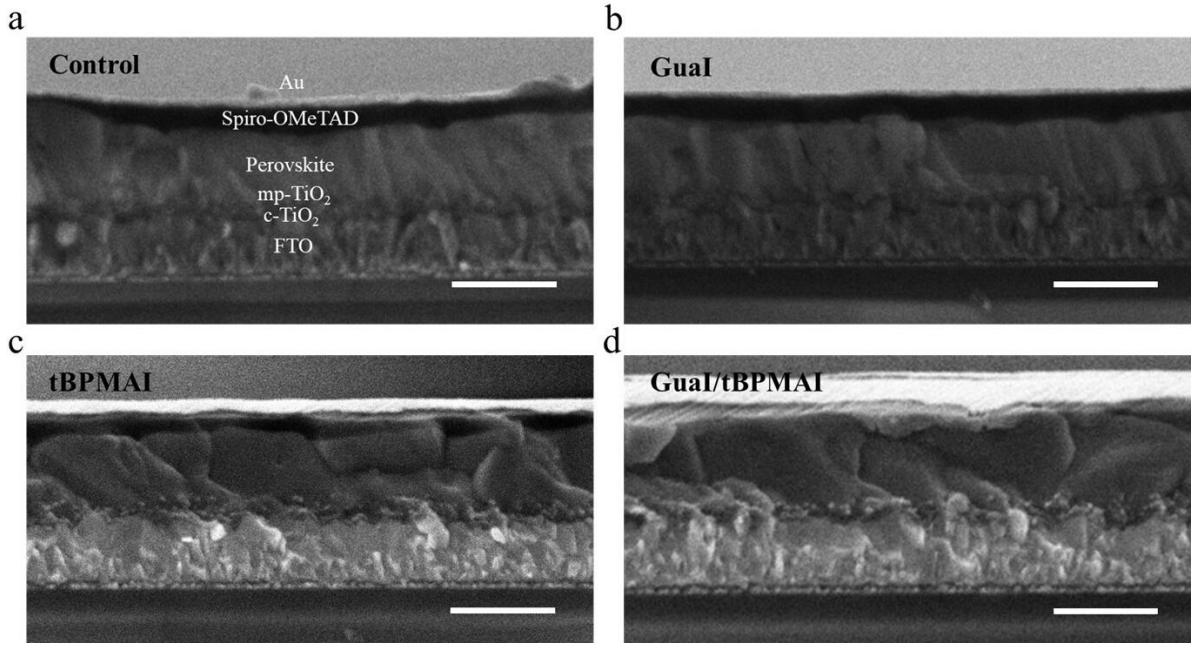

Fig. S22. Cross-sectional SEM images of the control (a), GuaI-treated (b), tBPMAI-treated (c), and GuaI/tBPMAI-treated (d) devices . Scale bar in the SEM images: 1 μm.

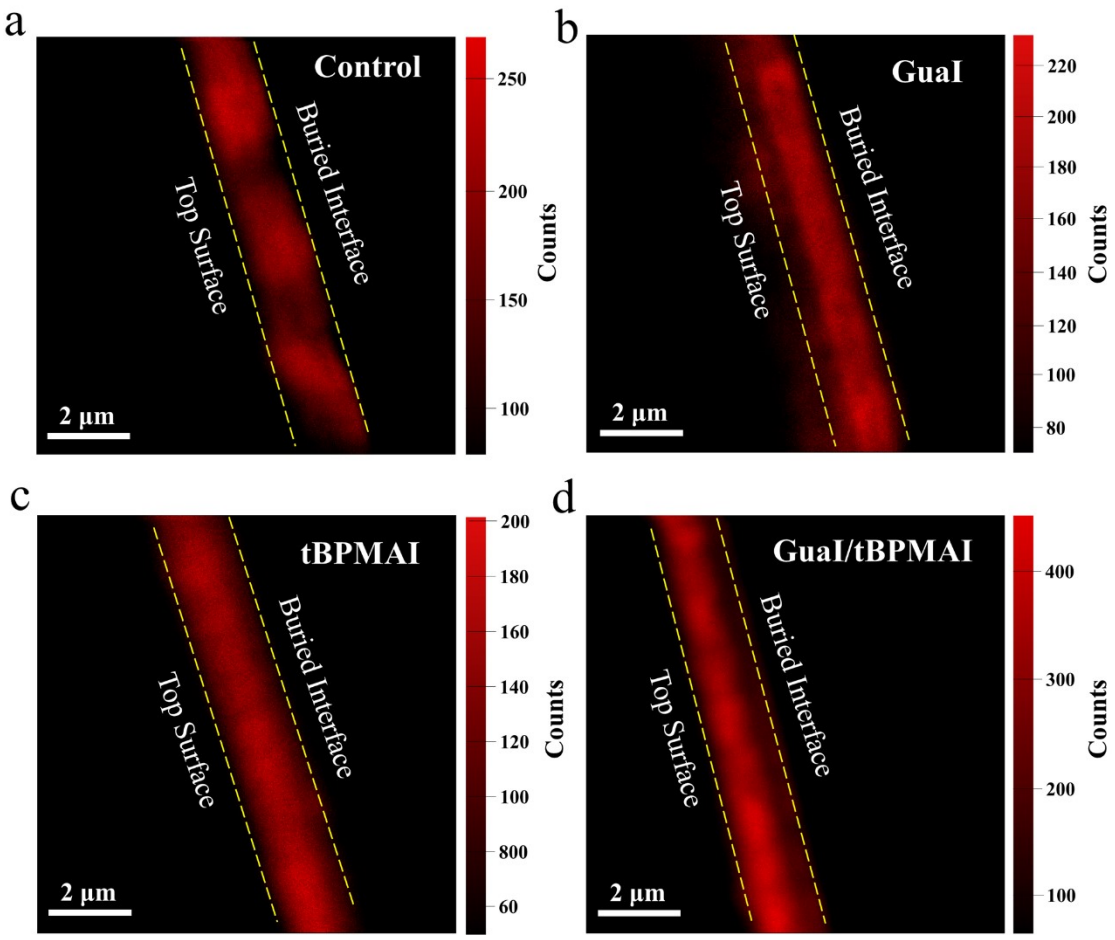

Fig. S23. (a-d) Cross-sectional confocal PL mapping images of the control (a), GuaI-treated (b), tBPMAI-treated (c), and GuaI/tBPMAI-treated (d) perovskite films. The perovskite films were deposited on FTO/c-TiO_2/m-TiO_2 substrates. The bright red areas represent PL emission from the perovskite film cross-sections. The yellow dot lines indicate the interfaces of the perovskite films.

Table S1. The photovoltaic parameters of the control, unitary GuaI (~1.67 mg/ml), unitary tBPMAI (~3.33 mg/ml) and binary GuaI/tBPMAI-treated PSCs based on various mass ratios, which were measured from 1.22 V to -0.02 V under the simulated AM1.5 G solar irradiation with the intensity of 100 m W cm^{-2}.

Sample	V_{OC} (V)	FF	J_{SC} (mA cm^{-2})	PCE (%)
Control	1.078	78.32	25.81	21.79%
GuaI/tBPMAI (0:1)	1.129	81.13	25.75	23.59%
GuaI/tBPMAI (1:0)	1.130	80.87	25.84	23.61%
GuaI/tBPMAI (1:1)	1.133	81.14	25.77	23.69%
GuaI/tBPMAI (1:2)	1.147	82.14	25.86	24.36%
GuaI/tBPMAI (2:1)	1.135	80.96	25.83	23.73%
GuaI (1.67 mg/ml)	1.099	78.35	25.80	22.21%
tBPMAI (3.33 mg/ml)	1.111	80.06	25.84	22.98%

Table S2. The decay curves are fitted according to the formula: $y = A_1e^{-x1/\tau1} + A_2e^{-x2/\tau2} + B$. Carrier lifetimes are calculated by the formula: $\tau_{ave} = \sum A_i\tau_i^2/\sum A_i\tau_i$. The detailed TRPL fitting parameters are shown in the following table.

Sample	τ_1 [ns]	τ_2 [ns]	A_1	A_2	τ_{ave} [ns]	R^2
Control	622.99	238.7	0.686	0.503	538	0.988
MAI	794.16	56.75	0.935	1.654	711	0.994
FAI	475.53	1109	0.819	0.410	817	0.989
EAI	1435.33	38.676	0.532	11.268	927	0.990
GuaI	1327.25	334.40	0.752	10.22	990	0.990
PEAI	2229.5	50.81	0.603	29.49	1081	0.989
tBPMAI	292.43	1245.99	0.196	0.831	1196	0.974
EAI/PEAI	1445.75	298.48	0.546	0.576	1240	0.987
GuaI additive	176.54	835.79	0.404	0.885	778	0.994
GuaI additive + tBPMAI	525.65	1591.28	0.290	0.620	1448	0.949
GuaI/tBPMAI	63.12	1826.31	2.04	0.724	1670	0.988

Table S3. The photovoltaic parameters of the control and binary EAI/PEAI-treated PSCs, which are measured from 1.22 V to -0.02 V under the simulated AM1.5 G solar irradiation with the intensity of 100 mW cm^{-2}.

Sample	V_{OC} (V)	FF	J_{SC} (mA cm^{-2})	PCE (%)
Control	1.077	78.63	25.83	21.87%
EAI	1.112	80.27	25.81	23.04%
PEAI	1.122	80.59	25.75	23.28%
EAI/PEAI	1.144	81.56	25.86	24.13%

Supplementary References

[1] H. Min, M. Kim, S.-U. Lee, H. Kim, G. Kim, K. Choi, J. H. Lee, S. I. Seok, *Science* **2019**, *366*, 749.